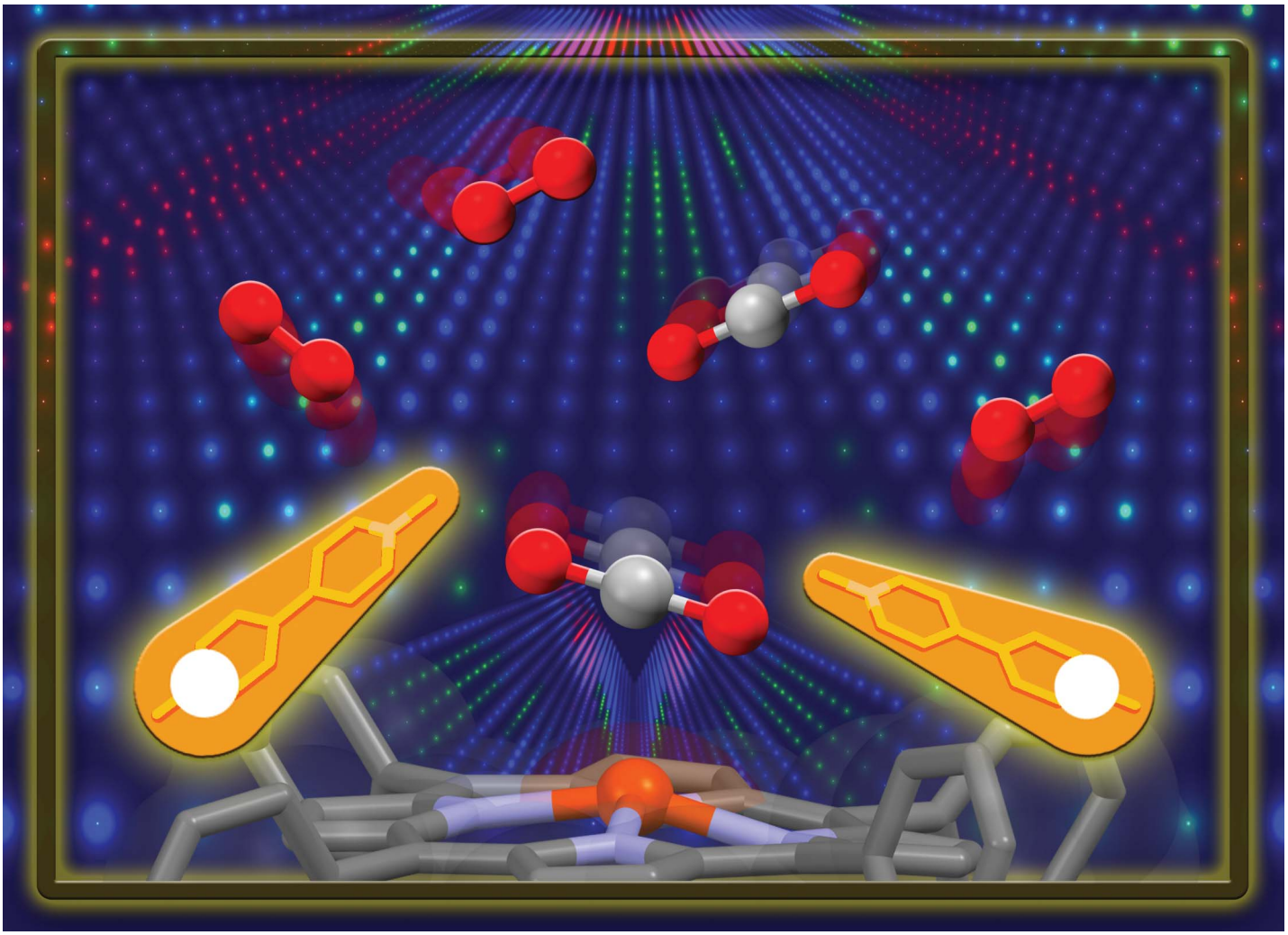

**Showcasing research from the team of Dr. Philipp Gotico (French Alternative Energies and Atomic Energy Commission) and Professor Ally Aukauloo (University of Paris Saclay) in collaboration with Max Planck Institute for Chemical Energy Conversion.**

Iron porphyrin flanked by viologen redox units for persistent carbon dioxide reduction in the presence of oxygen

We engineered an iron porphyrin catalyst incorporating viologen units to sustain $CO_2$ reduction under aerobic conditions. The viologens divert $O_2$ reduction, allowing the iron porphyrin core to selectively convert $CO_2$. While both redox sites act independently in solution, their integration on carbon nanotubes enabled 62% CO faradaic efficiency in 5% $O_2$, vastly outperforming the unmodified catalyst. This disparity between homogeneous and heterogeneous systems underscores how the reaction environment, interfacial structure, and electron transfer kinetics critically govern catalytic behavior.

Image reproduced by permission of Philipp Gotico from, *Chem. Sci.*, 2025, **16**, 20833.

## As featured in:


See Philipp Gotico, Ally Aukauloo *et al.*, *Chem. Sci.*, 2025, **16**, 20833.

ROYAL SOCIETY OF CHEMISTRY

15 YEARS ANNIVERSARY

rsc.li/chemical-science

Registered charity number: 207890

Chemical Science

ROYAL SOCIETY OF CHEMISTRY

EDGE ARTICLE

View Article Online
View Journal | View Issue



Cite this: *Chem. Sci.*, 2025, **16**, 20833

All publication charges for this article have been paid for by the Royal Society of Chemistry



# Iron porphyrin flanked by viologen redox units for persistent carbon dioxide reduction in the presence of oxygen

Haroon Rashid, [a] Diana Dragoe, [b] Atanu Rana, [c] Serena DeBeer, [c] Philipp Gotico, *[a] Winfried Leibl [a] and Ally Aukauloo *[b]

The electrocatalytic reduction of $CO_2$ to energy-rich forms such as CO or hydrocarbons is typically realized with pure $CO_2$. This is primarily to exclude $O_2$, which is a far better oxidant and a major competitor upon reduction of the $CO_2/O_2$ feed gas. Furthermore, the presence of $O_2$ can deactivate the catalytic material and reduce its effectiveness for $CO_2$ reduction. To confront this major challenge, different strategies are being pursued. We utilize a molecular design approach by adjoining to a known catalyst a redox active module that can competitively divert the deleterious $O_2$ activity. We tailored an iron porphyrin, a prominent catalyst for $CO_2$ reduction, flanked by viologen units known for their efficient $O_2$ reduction. Electrochemical studies on the homogeneous phase of the pre-catalyst, the iron(III)-μ-oxo form, show the independent activity of both modules. When heterogenized with carbon nanotubes on a carbon paper electrode, we found that the catalyst could sustain the aerobic (5% $O_2$) reduction of $CO_2$ to CO with a faradaic efficiency of 62%, while the activity of the unmodified iron porphyrin fell to 18% under the same experimental conditions.

Received 13th April 2025
Accepted 1st October 2025

DOI: 10.1039/d5sc02722e

rsc.li/chemical-science

## Introduction

There is ample agreement that the electrocatalytic reduction of carbon dioxide ($CO_2$), using renewable energy sources, is a sustainable pathway to mitigate the ever-increasing $CO_2$ level in the atmosphere caused by our fossil fuel-based economy.[1] The $CO_2$ molecule lies in an energetic well and its conversion to reduced forms of carbon necessitates the use of catalysts.[2,3] Presently, there is a great effort focused on finding new catalytic materials for the selective $CO_2$ reduction reaction ($CO_2$RR). While this research is advancing, another important challenge must be addressed – the unavoidable presence of $O_2$ in all $CO_2$ sources.[4] The reduction of $CO_2$ in the presence of $O_2$ is problematic as the latter is a far better oxidant and ultimately leads to inactivation of the catalytic system.[5,6] Even for concentrated sources of $CO_2$, such as flue gases, the level of $CO_2$ reaches up to 15% with an $O_2$ content of *ca.* 3–5%.[4] If $CO_2$ is to be purified, a massive amount of energy would be necessary based on the actual $CO_2$ alkanolamine capture processes.[7,8] Therefore, it will be highly desirable if $CO_2$ from concentrated sources such as flue gases could be directly used without further pre-separation steps. Chemists are taking different tracks to address this complicated scientific dilemma (Scheme 1).

Berlinguette and colleagues have recently reported an ingenious way to overcome this issue by delivering high local

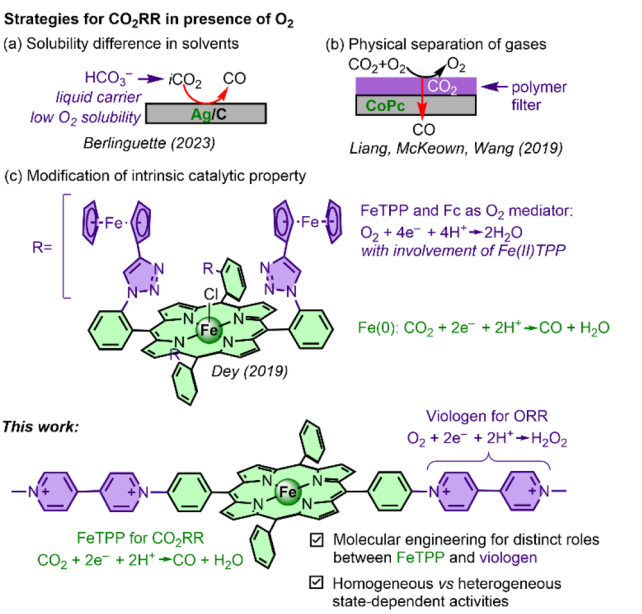


Scheme 1 Strategies for the electrocatalytic $CO_2$RR in the presence of oxygen.

[a]*Institut de Biologie Intégrative de la Cellule (I2BC), Institut des Sciences du Vivant Frédéric-Joliot, CEA Saclay, 91191, Gif-sur-Yvette, France. E-mail: philipp.gotico@cea.fr*

[b]*Institut de chimie Moléculaire et des Matériaux d'Orsay (ICMMMO), Université Paris-Saclay, 91405, Orsay, France. E-mail: ally.aukauloo@universite-paris-saclay.fr*

[c]*Max Planck Institute for Chemical Energy Conversion, D-45470 Mülheim an der Ruhr, Germany*

concentration of $CO_2$ at a composite Ag/C cathode using aqueous bicarbonate solutions as the $CO_2$ carrier.[7] The authors found that the concentration of $O_2$ at the cathode is comparatively low due to its low solubility in water, hence favoring the reduction of the overwhelming amount of $CO_2$. 65% selectivity for the $CO_2$ to CO reduction was observed using bicarbonate, while it dropped by more than 90% when $CO_2$ gas was used. Wang and colleagues have proposed another route, whereby the concentration of $O_2$ was decreased at the surface of a hybrid gas diffusion electrode constituting a cobalt phthalocyanine molecular catalyst covered with a polymer selective for $CO_2$ transport.[9] A faradaic efficiency (FE) of 76% for CO production was reported with 5% $O_2$ content in the $CO_2$ gaseous feed. In the absence of the polymer, the $FE_{CO}$ collapsed to zero in the presence of 5% $O_2$. This report remains the sole example of investigating the effect of $O_2$ on $CO_2$ reduction when discrete molecular catalysts are adsorbed onto a carbon-based electrode.

Recently, a covalent organic framework (COF) was developed by Huang and colleagues, which features a nickel phthalocyanine interconnected by a Robson biscompartmental-type ligand with two cobalt(II) ions.[10] This system was found to be $O_2$-tolerant, as suggested by the authors. Notably, the authors proposed that a cobalt-bound *OOH species facilitates $CO_2$ reduction by interacting with an adjacent cobalt-bound *COOH. This proposed reactivity pattern was primarily supported by theoretical calculations, while the role of NiPc in the aerobic $CO_2$ catalysis was not addressed. Interestingly, although both the oxygen reduction reaction (ORR) and $CO_2$RR occur concurrently, the observed enhancement in current density during electrocatalysis was solely attributed to the $CO_2$RR, therefore leaving open the question on the efficacy of the ORR occurring at the dicobalt site.

Dey and coworkers were the first to tackle this issue from a completely molecular approach.[6] In their strategy, the authors used an iron porphyrin, known as one of the best molecular catalysts for $CO_2$ reduction to CO, and covalently tethered four ferrocene (Fc) units. Upon reaching the Fe(II) state, $O_2$ binds and shares one electron with the iron center, and three of the Fc units each contribute one electron to convert $O_2$ to $H_2O$. In this scenario, the iron porphyrin is itself implicated in the ORR.[11] In the presence of $CO_2$, another catalytic wave was observed at more negative potential typical for the catalytic $CO_2$ reduction by an iron porphyrin. Interestingly, the authors have shown that the formal Fe(0) species is far more reactive with $CO_2$ than with $O_2$.[6] Hence, in the presence of $O_2$ and in the Fe(0) state, the reduction of $CO_2$ prevails. A CO selectivity of 84% was reported for bulk electrolysis in a homogeneous phase and in the presence of 25% $O_2$ volume fraction.

We have been interested in investigating $CO_2$ reduction in the presence of $O_2$ with a designed molecular catalyst, an iron porphyrin flanked by two viologen units (Scheme 1). The choice for the viologen modules was guided by extensive literature on methyl viologen reactivity to reduce $O_2$ to form $H_2O_2$ at quite modest overpotential.[12–17] Hence, our line of thought is to divert the $O_2$ reduction to the viologen units, while the iron center should be the privileged site to deal with $CO_2$ reduction. The chemical structure of the targeted bimodular catalyst, iron diviologen phenyl porphyrin, in short, **FeDVPP**, is presented in Scheme 1. While this work was ongoing, a reticular framework with similar constitutive units was reported.[18] However, the redox properties of the constitutive units were not addressed leaving a gap in understanding how these units function in synergy to drive the $CO_2$ reduction in the presence of $O_2$.

In this study, we have chosen the μ-oxo-diiron(III) porphyrin dimer as the pre-catalyst form, denoted as $\mathbf{[(Fe^{III}DVPP)_2O]^{8+}}$ and hereby abbreviated as $\mathbf{(FeDVPP)_2O}$ (Scheme 2). For simplicity, we will specify the oxidation states of the iron center and the viologen units only when discussing redox events. Several reasons prompted us to base this study on the dimer. First, from a synthetic standpoint, the dimer was more readily isolated following the classic metalation procedure. This approach also facilitated the exchange of the accompanying anions, which was beneficial for solubility reasons. The choice for choosing the dimer is also based on a comprehensive study by Kadish *et al.* on the μ-oxo-diiron(III) tetraphenyl porphyrin.[19] They demonstrated that the electrochemical events of the $Fe^{III/II}$ couple of the μ-oxo-diiron(III) tetraphenyl porphyrin occurred at more cathodic potentials. This shift should effectively be beneficial to separate the redox events of the iron porphyrins and the viologen units that occur at a more positive potential window. Additionally, previous studies argued that using μ-oxo-diiron(III) porphyrin is advantageous for heterogeneous catalysis compared to its monomeric derivative.[20–22] This is because the reduction and exclusion of the oxo bridge results in the formation of two closely positioned monomeric iron porphyrins, enabling cooperative catalysis. This structural arrangement can possibly enhance $CO_2$ activation[23] when adsorbed onto the electrode surface during heterogeneous catalysis. We found here that $\mathbf{(FeDVPP)_2O}$ can indeed lead to the active form of the catalyst, *i.e.*, $\mathbf{Fe^0DVPP}$, to perform the reduction of $CO_2$ in the presence of $O_2$, maintaining good $FE_{CO}$ and CO partial current density compared to an iron tetraphenyl porphyrin (**FeTPP**) when heterogenized on the carbon nanotube/carbon paper electrode.[24] In what follows, we bring elements to support this original electrocatalytic activity for the $CO_2$ reduction while concomitantly accommodating the $O_2$ reduction. This study represents a rare example of a heterogenized molecular complex for aerobic $CO_2$ reduction that importantly touches on differences that arise from homogeneous and heterogeneous states of the system.

## Results and discussion

The catalyst $\mathbf{(FeDVPP)_2O}$ was synthesized by treatment of an iron *para*-diaminophenyl porphyrin with methylated Zincke salt, as

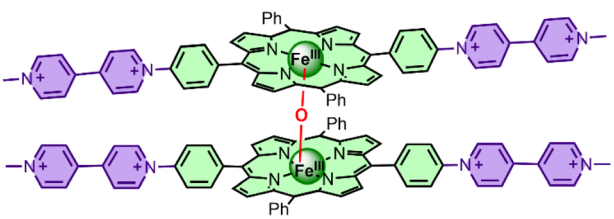


Scheme 2 Chemical structure of μ-oxo-diiron(III) diviologen phenyl porphyrin $[(Fe^{III}DVPP)_2O]^{8+}$.

detailed in the SI (Fig. S1–S3). The precursors and the final compound were characterized by nuclear magnetic resonance (NMR) spectroscopy, electrospray ionization high-resolution mass spectrometry (ESI-HRMS), matrix-assisted laser desorption/ionization time-of-flight (MALDI-TOF) mass spectrometry, electron paramagnetic resonance (EPR) spectroscopy, and UV-visible spectroscopy (Fig. S4–S23). In contrast to the high spin Fe(III) EPR spectrum typically observed for iron porphyrins, the **(FeDVPP)$_2$O** complex is EPR silent due to the antiferromagnetic coupling of two high spin Fe(III) centers (Fig. S24).

### Electrochemical characterization

The electrochemical properties of **(FeDVPP)$_2$O** were studied using cyclic voltammetry (CV) and differential pulse voltammetry (DPV) in Ar-saturated dry dimethylformamide (DMF) and compared to reference compounds for redox state attributions (Fig. 1, potentials are summarized in Table S1). The first two redox waves of **(FeDVPP)$_2$O** (I and II in Fig. 1) at −0.24 V and −0.63 V *vs.* SCE can be attributed to the consecutive one-electron reduction of the four viologen units, $V^{2+/+}$ and $V^{+/0}$, respectively.

(I): $[(\mathbf{DV^{2+}PP})\mathbf{Fe^{III}}\text{–O–}\mathbf{Fe^{III}}(\mathbf{DV^{2+}PP})]^{8+} + 4e^- \rightarrow [(\mathbf{DV^{+}PP})\mathbf{Fe^{III}}\text{–O–}\mathbf{Fe^{III}}(\mathbf{DV^{+}PP})]^{4+}$ $E = -0.24$ V

(II): $[(\mathbf{DV^{+}PP})\mathbf{Fe^{III}}\text{–O–}\mathbf{Fe^{III}}(\mathbf{DV^{+}PP})]^{4+} + 4e^- \rightarrow [(\mathbf{DV^{0}PP})\mathbf{Fe^{III}}\text{–O–}\mathbf{Fe^{III}}(\mathbf{DV^{0}PP})]^{0}$ $E = -0.63$ V

These peaks are anodically shifted by 210 mV and 180 mV, respectively, compared to methyl viologen (**MV**) (Fig. 1a and Table S1). The free base porphyrin, **H$_2$-DVPP**, shows a similar anodic shift (Fig. S25 and Table S1) indicating the dissymmetric nature of the viologen units in the presence of a phenyl group, instead of a methyl group, on one of the nitrogen atoms. Of note, the appearance of only two waves for the four viologen units shows that they are not electronically coupled in **(FeDVPP)$_2$O**.

The redox waves (III to V) at −1.07 V, −1.45 V, and −1.68 V match with the reduction events of the μ-oxo-iron tetraphenyl porphyrin dimer, as initially reported by Kadish and colleagues.[19] Redox peak III corresponds to the proton-coupled reduction of the Fe(III)–O–Fe(III) motif to generate Fe(II) and Fe(II)–OH and the reduction of Fe(II) to Fe(I); peak IV corresponds to the proton-coupled reduction of Fe(II)–OH to Fe(I); and peak V corresponds to the reduction of Fe(I) to formal Fe(0).

(III): $[(\mathbf{DV^{0}PP})\mathbf{Fe^{III}}\text{–O–}\mathbf{Fe^{III}}(\mathbf{DV^{0}PP})]^{0} + 2e^- + H^+ \rightarrow [(\mathbf{DV^{0}PP})\mathbf{Fe^{II}}]^{0} + [(\mathbf{DV^{0}PP})\mathbf{Fe^{II}}\text{–OH}]^-$ $E = -1.07$ V

$[(\mathbf{DV^{0}PP})\mathbf{Fe^{II}}]^{0} + e^- \rightarrow [(\mathbf{DV^{0}PP})\mathbf{Fe^{I}}]^-$ $E = -1.07$ V

(IV): $[(\mathbf{DV^{0}PP})\mathbf{Fe^{II}}\text{–OH}]^- + e^- + H^+ \rightarrow [(\mathbf{DV^{0}PP})\mathbf{Fe^{I}}]^- + H_2O$ $E = -1.45$ V

(V): $[(\mathbf{DV^{0}PP})\mathbf{Fe^{I}}]^- + e^- \rightarrow [(\mathbf{DV^{0}PP})\mathbf{Fe^{0}}]^{2-}$ $E = -1.68$ V

Further evidence for the attribution of the redox states comes from the CV and DPV of the monomer **FeDVPP** prepared by HCl treatment of an organic solution of the dimer. As anticipated, the electrochemical response of the monomer **Fe$^{III}$DVPP** (red curves in Fig. 1) is marked by the presence of a new redox wave at −0.14 V that can be assigned to the $Fe^{III/II}$ couple prior to the electrochemical response of the viologen units at −0.31 V and −0.64 V (Fig. 1 and Table S1). This is a clear indication that once the monomeric form of **Fe$^{II}$DVPP** is formed, the subsequent reduction processes concern the addition of electrons on the viologen units, followed by the typical porphyrin-centered redox waves.

To gain insight into the electronic structure of the **Fe$^{II}$DVPP** species and identify the site for the subsequent addition of two electrons, we performed DFT calculations. Our results primarily support a metal-centered description for the Fe(II) state,[29] with no significant contribution from the oxidized viologen units. Interestingly, we found that the Fe(II) complex is more stable by approximately 8 kcal mol$^{-1}$ in an intermediate spin state (S = 1), compared to both the high spin (S = 2) and low spin (S = 0) states (see Table S9 and Fig. S44). Fig. 2a portrays the optimized structure of $[(\mathbf{DV^{2+}PP})\mathbf{Fe^{II}}]^{4+}$.

As observed, the phenyl rings connecting the porphyrin ring to the viologen units are tilted towards the porphyrin plane and the viologen units and calculated to be at an angle of approximately 70° with the porphyrin plane. Upon addition of two electrons, the optimized structure reveals a flattening of the two viologen units, with the dihedral angle between the two pyridyl rings of the **MV** unit decreasing from 12.3° for $[(\mathbf{DV^{2+}PP})\mathbf{Fe^{II}}]^{4+}$ to 1.4° for $[(\mathbf{DV^{+}PP})\mathbf{Fe^{II}}]^{2+}$. These structural changes are consistent with the one-electron reduction of the viologen units,

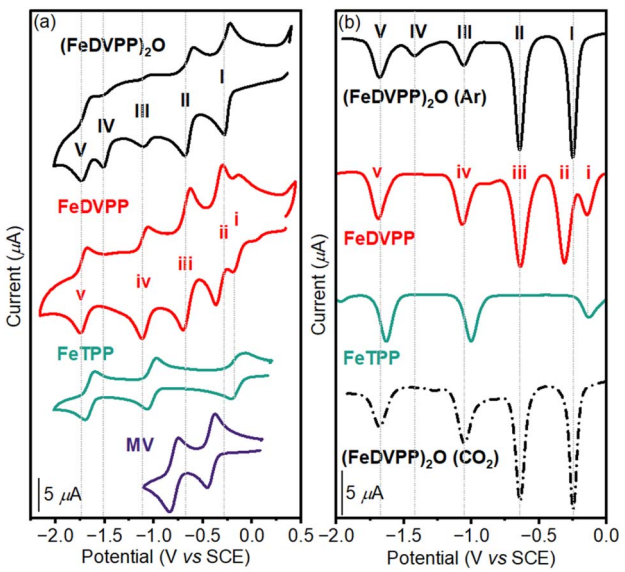


Fig. 1 (a) Cyclic voltammograms of 0.25 mM **(FeDVPP)$_2$O** (black), 0.5 mM **FeDVPP** (red), 0.5 mM **FeTPP** (green), and 0.5 mM **MV** (purple) in DMF with 0.1 M $[Bu_4N]PF_6$ under Ar at 100 mV s$^{-1}$ scan rate. (b) Differential pulse voltammograms of **(FeDVPP)$_2$O** (black), **FeDVPP** (red) and **FeTPP** (green) in Ar, and **(FeDVPP)$_2$O** in $CO_2$ (dash dot) [E step: 4 mV, amplitude: 50 mV, pulse width: 60 ms, sampling width: 20 ms, and pulse period: 500 ms].

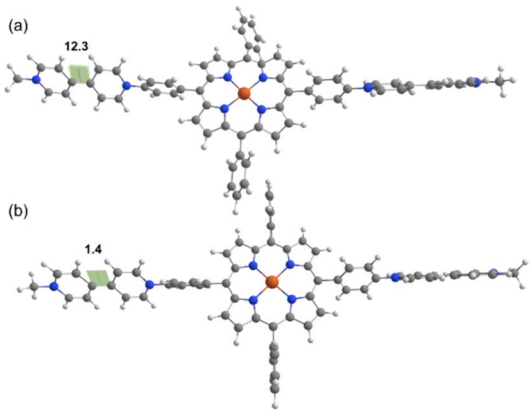


Fig. 2 Structural and electronic changes computed for (a) $[(DV^{2+}PP)Fe^{II}]^{4+}$ and (b) the corresponding two-electron reduced form best described as uncoupled two radical cations of the viologen and the $Fe^{II}$ porphyrin, $[(DV^{+}PP)Fe^{II}]^{2+}$. Numbers denote dihedral angles between pyridyl rings of viologen.

resulting in a conjugated radical cation form of the viologen.[30] No significant structural modifications are observed for the iron porphyrin, where the iron remains in the Fe(II) state and maintains an intermediate spin state. The calculated Mulliken charge and spin density distribution between the viologen and Fe–porphyrin center indicate minimal electronic coupling between the components. Following the one-electron reduction of each viologen, 97% of the one-electron spin density is localized on the individual viologen unit (Table S9). An interesting finding is the resulting ground spin state for $\mathbf{[(DV^{+}PP)Fe^{II}]^{2+}}$ where both the quintet and triplet states are equally stabilized. However, the orientation of the phenyl linking the porphyrin and the viologen units seems to regulate this magnetic exchange (Fig. S44). Further DFT calculations are needed to explore the electronic structure of such further reduced and relevant forms, which is outside the current scope of the study.

(i): $\mathbf{[(DV^{2+}PP)Fe^{III}]^{5+}} + e^- \rightarrow \mathbf{[(DV^{2+}PP)Fe^{II}]^{4+}}$ $E = -0.14$ V

(ii): $\mathbf{[(DV^{2+}PP)Fe^{II}]^{4+}} + 2e^- \rightarrow \mathbf{[(DV^{+}PP)Fe^{II}]^{2+}}$ $E = -0.31$ V

(iii): $\mathbf{[(DV^{+}PP)Fe^{II}]^{2+}} + 2e^- \rightarrow \mathbf{[(DV^{0}PP)Fe^{II}]^{0}}$ $E = -0.64$ V

(iv): $\mathbf{[(DV^{0}PP)Fe^{II}]^{0}} + e^- \rightarrow \mathbf{[(DV^{0}PP)Fe^{I}]^{-}}$ $E = -1.06$ V

(v): $\mathbf{[(DV^{0}PP)Fe^{I}]^{-}} + e^- \rightarrow \mathbf{[(DV^{0}PP)Fe^{0}]^{2-}}$ $E = -1.68$ V

In addition to the appearance of redox peak i corresponding to $(DVPP)Fe^{III/II}$, the absence of redox peak IV [reduction of Fe(II)–OH to Fe(I)] in the **FeDVPP** monomer is a contrasting difference with that of the $\mathbf{(FeDVPP)_2O}$ dimer. Curious as to how the dimer breaks under eventual electrocatalytic conditions (presence of a proton co-substrate and a $CO_2$ substrate), CV of $\mathbf{(FeDVPP)_2O}$ was performed by adding trifluoroethanol (TFE) in Ar-saturated dry DMF (Fig. S26a), and in another experiment, $CO_2$ was added to a dry DMF solution without a proton source (Fig. 1b and S26b). Under these conditions, we again observed the disappearance of peak IV, but the redox peak i was not observed. This indicates that the presence of TFE as a weak acid and traces of carbonic acid (possibly formed from traces of $H_2O$ in $CO_2$-saturated dry DMF) are not sufficient to cleave $\mathbf{(FeDVPP)_2O}$, but additionally a reducing condition (<−1.07 V) is required to fully cleave the dimer.

## Catalysis under homogeneous conditions

In the presence of both $CO_2$ and TFE (Fig. 3a and S27), catalytic currents are observed in the Fe(I/0) redox state for both $\mathbf{(FeDVPP)_2O}$ and **FeTPP** (serving as the reference). At the same metal ion concentration, both complexes exhibit equally high catalytic currents and similar onset potentials, suggesting that the additional viologen units do not directly influence the $CO_2$ reduction activity. Furthermore, the results also indicate that under catalytic and reducing homogeneous conditions, the dimer configuration, as previously discussed, is not the active catalytic form. Instead, it is the **FeDVPP** monomer formed after cleavage of the μ-oxo bond that predominantly drives the catalysis.

We then probed the reactivity of the $\mathbf{(FeDVPP)_2O}$ catalyst in the presence of $O_2$ and TFE (Fig. 3b). We observed a catalytic current after the first reduction wave of the viologen units at −0.63 V, with an onset potential at −0.48 V. This contrasts with methyl viologen where catalysis is already observed on the first reduction wave at −0.45 V (Fig. 3b). This change in reactivity may be attributed to the less reducing power of the singly reduced viologen units of $\mathbf{(FeDVPP)_2O}$ (−0.24 V) requiring an onset potential of −0.48 V to start $O_2$ reduction. The mechanism for the reduction of $O_2$ with **MV** has been reported to produce $H_2O_2$,[17] as noted in previous studies. This has also been supported by the group of Compton in the context of heterogeneous electrocatalysis.[13] Their work further confirms the role of **MV** in facilitating the formation of $H_2O_2$ during the reduction of $O_2$ in various catalytic systems.

The same mechanism is expected to play for the viologen units in $\mathbf{(FeDVPP)_2O}$, albeit occurring at more negative potential. Notably, this reduction occurs well before the background oxygen reduction at the glassy carbon (GC) electrode, which takes place at a peak potential of −0.89 V (Fig. S29), highlighting

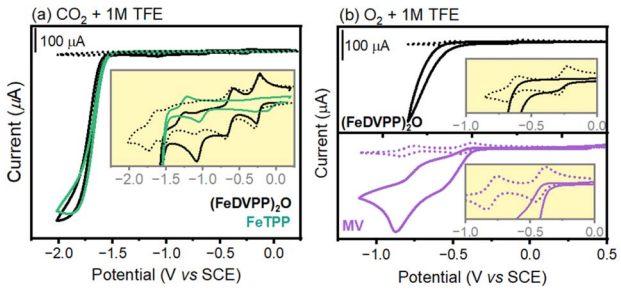


Fig. 3 Cyclic voltammograms of 0.25 mM $\mathbf{(FeDVPP)_2O}$ (black) in DMF with 0.1 M $[Bu_4N]PF_6$ and 1 M trifluoroethanol (TFE) under (a) $CO_2$ and (b) $O_2$, in comparison to 0.5 mM **FeTPP** (green) and 0.5 mM **MV** (purple). Dotted curves show CV curves recorded in Ar-saturated DMF. Insets show zoomed data.

the significant role of the viologen units in the ORR. Furthermore, as discussed above, using TFE as a proton source only cleaves the μ-oxo **(FeDVPP)$_2$O** dimer at <−1.07 V to generate the Fe(II) state. This is almost 600 mV after the observed onset of the ORR, indicating that under our experimental conditions the iron center does not intervene in the ORR at these early potentials under the CV timescale. Noteworthily, for Dey's iron porphyrin catalyst bearing Fc units, the ORR was observed after reaching the Fe(II) state, with the aid of three electrons from the ferrocene units to realize the reduction of $O_2$ to $H_2O$.[6]

The electrocatalytic properties of iron porphyrin catalysts for $CO_2$ reduction under anaerobic conditions are well established, positioning it as one of the most efficient molecular catalysts. It has also been widely studied for its ability to catalyze the reduction of $O_2$.[11] However, the $O_2$ reduction process typically occurs first due to its more favorable thermodynamics, while the $CO_2$ reduction takes place at more negative potential. Therefore, we interrogated the electrocatalytic behavior of **(FeDVPP)$_2$O** and **FeTPP** for $CO_2$ reduction in the presence of controlled amounts of $O_2$ with TFE as the proton source (Fig. 4 and S30). This should provide insightful information on the competitive multi-electron and multi-proton catalysis for both concomitant processes.

With **FeTPP** as the catalyst, $O_2$ was reduced at −0.86 V *vs.* SCE by Fe(II), and its onset potential for the $CO_2$RR appears at −1.62 V, close to the value for Fe(I/0) at −1.64 V (Fig. 4a). Controlled potential electrolysis was performed at −1.75 V *vs.* SCE both under anaerobic and aerobic conditions (5% $O_2$) to measure the efficiency at which CO is produced (Fig. 4b). We found that for each set of experiments $H_2$ production was minimal with a $FE_{H_2}$ of 0.5% and 1%, while the $FE_{CO}$ dropped from 80% to 49%, respectively. Importantly, the fall in the $FE_{CO}$ was accompanied by an ORR with a calculated $FE_{ORR}$ of *ca.* 16%, considering the unique two-electron two-proton reduction product, $H_2O_2$. A recent extensive investigation of an iron porphyrin for $O_2$ reduction by Surendranath and colleagues,[25] using a rotating ring disk electrode, however, points to only a partial reduction of $O_2$ to $H_2O_2$ in DMF (27%). Henceforth, our reported value for the $FE_{ORR}$ is likely biased, meaning that the actual amount of $H_2O_2$ produced is less than what would be expected from the complete conversion of $O_2$ to $H_2O_2$. The decrease in efficiency for the $CO_2$ to CO reduction in the presence of 5% $O_2$ can be explained by the redirection of some of the reduced **Fe$^{II}$TPP** species to perform the ORR, limiting their availability to participate in the $CO_2$ reduction process.

With the **(FeDVPP)$_2$O** catalyst, $O_2$ was first reduced at −0.64 V by its viologen units, and an onset catalytic wave for the $CO_2$RR appears at −1.54 V, prior reaching Fe(I/0) at −1.68 V (Fig. 4a). Notably, the presence of $CO_2$ does not influence the redox properties of the viologen modules, as evidenced by the lack of change of the onset potential for the $O_2$ catalytic reduction process. Interestingly, we see a noticeable anodic shift of the onset for the $CO_2$RR with **(FeDVPP)$_2$O** (Fig. S30) in comparison of both **(FeDVPP)$_2$O** and **FeTPP** when the catalysis was performed with pure $CO_2$ feed gas (Fig. 3a). At this time, we do not have a clear understanding for this >100 mV shift to more positive values for the onset potential of $CO_2$RR. One hypothesis for the earlier activation of $CO_2$ could be related to the intrinsic ORR activity of the viologens units. It is therefore possible that unaccounted side reactions such as superoxide, generated from the reduction of $O_2$ by the singly reduced viologen unit, reacting with $CO_2$, or changes in reaction intermediates are playing a role. Further investigation into these aspects might help clarify the reasons behind this unexpected shift.[26–28]

Controlled potential electrolysis of **(FeDVPP)$_2$O** at −1.75 V shows a decrease in $FE_{CO}$ from 55% to 3% when introducing 5% $O_2$ (Fig. 4b and S30a). This is concomitant with the considerable increase of the ORR activity (35%) based on the amount of $O_2$ consumed from GC measurements. Since the ORR products ($H_2O_2$ and/or $H_2O$) are difficult to quantify under our operating conditions, we have taken $O_2$ consumption as a key metric to follow the ORR with the following expected FE range: minima assuming 2e$^-$ reduction, while maxima shown as a gray line assuming 4e$^-$ reduction. From this range, the missing FE might possibly come from further reduction of $H_2O_2$ to $H_2O$. We further investigated this aspect by performing CV of **(FeDVPP)$_2$O** with the addition of an aqueous solution of $H_2O_2$ (Fig. S31) and noticed a catalytic process at −0.35 V, describing the further reduction of $H_2O_2$ to water.

Based on the above experiments under homogeneous conditions, we clearly observed a much more dominant ORR and significantly reduced $CO_2$RR activity for **(FeDVPP)$_2$O** than **FeTPP**. This can be attributed to the bifunctional roles of the reduced viologen units and reduced iron porphyrin in **(FeDVPP)$_2$O** in constant competition toward the ORR and $CO_2$RR. We have identified relevant intermediates of the **(FeDVPP)$_2$O** catalyst (see Section E of the SI). Bulk electrolysis experiments with lower concentration of the catalyst (Fig. S32c) showed no significant difference, hinting that an intramolecular process, such as internal electron transfer between the constitutive units of the **(FeDVPP)$_2$O** catalyst, might play a significant role, especially since this stands as a contrasting difference to the nonmodified **FeTPP**, where no such intramolecular process can occur. The outcomes of electrocatalytic

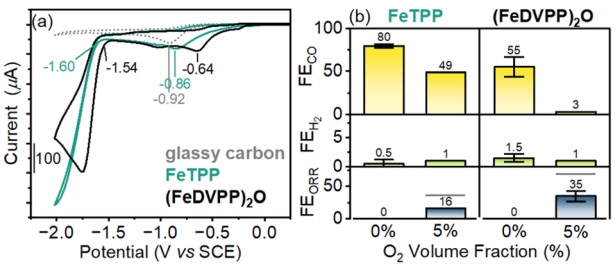


Fig. 4 (a) Cyclic voltammograms of 0.25 mM **(FeDVPP)$_2$O** (black) and 0.5 mM **FeTPP** (green) in DMF with 0.1 M $[Bu_4N]PF_6$ and 1 M trifluoroethanol (TFE) under $CO_2$ with 20% $O_2$. The dotted gray curve represents the response of glassy carbon. (b) Faradaic efficiency (FE) for CO, $H_2$, and the ORR at different $O_2$ volume fractions (in the $CO_2$ + $O_2$ mixture) after 2 h of homogeneous electrolysis at −1.75 V *vs.* SCE in DMF with 0.1 M $[Bu_4N]PF_6$ and 1 M TFE. The ORR represents $O_2$ consumption assuming 2e$^-$ reduction (if 4e$^-$ occurs, the gray line is expected). Further data are provided in Fig. S32, S33 and Table S3.

experiments conducted under homogeneous conditions were, however, inconclusive in untangling the competing ORR and $CO_2$RR pathways for both catalysts under investigation. Taking into account the collected results from the homogeneous catalysis, it appears that a more detailed and profound investigation is warranted to understand the effect of $O_2$ on the $CO_2$ catalysis for the parent **FeTPP** and **(FeDVPP)$_2$O**. These studies fall outside the scope of the present report.

### Anaerobic $CO_2$RR catalysis under heterogeneous conditions

At this stage, we reasoned that one way to bypass such mechanistic intricacies in the homogeneous phase was to investigate the electrocatalytic properties in the heterogeneous phase. The recent reports on $CO_2$ reduction in the presence of $O_2$ have been realized in the heterogeneous phase, probably to shunt the complicated intertwined events undergoing in the homogeneous phase. In addition, by doing so, we can take leverage of the difference in $O_2$ and $CO_2$ solubility between homogeneous (DMF) and heterogeneous ($H_2O$) conditions, *i.e.*, lower $O_2$ concentration of 0.6 mM in water than 3 mM in DMF, while maintaining a relatively good concentration of $CO_2$ (34 mM in $H_2O$ and 230 mM in DMF). The actual concentration of dissolved oxygen in different solvents (0.5 M aqueous $KHCO_3$ *vs.* DMF) and ($O_2$/$CO_2$) gas feed ratios was estimated by quenching studies of the excited state of a Ru-pyridyl-type chromophore, as detailed in the SI (Section D). The results show a linear correlation between the ($O_2$/$CO_2$) gas feed ratio and dissolved oxygen, indicating that $O_2$ concentration can be effectively dropped down to 0.15 mM in DMF and 0.03 mM in 0.5 M $KHCO_3$ when using 5% $O_2$/$CO_2$ gas feed (Table S10).

The heterogenization of the catalysts was realized following previously reported procedures.[31–33] The iron porphyrins were immobilized on multi-walled carbon nanotubes (MWCNTs), and the corresponding ink was drop-cast on a carbon paper (CP) electrode (see the SI for details). A similar metal concentration of 52.5 nmol cm$^{-2}$ was maintained to have accurate comparison between **(FeDVPP)$_2$O** and **FeTPP**. The amount of electrochemically active catalyst on the surface of **(FeDVPP)$_2$O** and **FeTPP** modified CNT/CP electrodes was determined to be 1.69 and 3.92 nmol cm$^{-2}$, respectively, indicating very similar percentage of electroactive sites of 6.4% and 7.5%, respectively (Fig. S36 and Table S4). The immobilization of **(FeDVPP)$_2$O** on the surface of the modified electrode was supported by the presence of the redox waves of the viologen units that appear at 0.33 V and −0.18 V *vs.* RHE (Fig. S37b), which are anodically shifted by 320 mV and 200 mV, respectively, compared to **MV** (Fig. S37a),[34] as similarly observed under homogeneous conditions.

In the presence of $CO_2$, both **(FeDVPP)$_2$O** and **FeTPP** modified electrodes show current enhancement but with the earlier observed onset potential of −0.4 V *vs.* RHE for **(FeDVPP)$_2$O** (Fig. S37c and d). Controlled potential electrolysis within the potential range of −0.7 to −1 V *vs.* RHE in 0.5 M $KHCO_3$, show a compromise of CO selectivity and current density at −0.8 V for both **(FeDVPP)$_2$O** and **FeTPP** (Fig. 5a, S38 and Table S5). At this potential, **(FeDVPP)$_2$O** exhibited a $FE_{CO}$ (76%) and CO selectivity (96%) similar to **FeTPP**, but at a higher CO partial current density of 1.65 mA cm$^{-2}$ as compared to 1.00 mA cm$^{-2}$ respectively, as shown in Fig. 5b. When comparing the effective turnover frequency (eTOF) by normalizing to the electroactive sites, we see that **(FeDVPP)$_2$O** has a higher eTOF than **FeTPP** (Fig. S42). This indicates that the viologen units significantly increase the inherent $CO_2$RR activity of viologen-modified iron porphyrin on the surface of the electrode. This observation can be attributed to the role of the viologen units that can act as redox active modules, enhancing the electronic communication between the reduced viologen forms and the iron center and hence promoting the convoy of electrons to the active Fe center, similar to what had been observed by Cao and his associates when they integrated viologen groups into Co-porphyrin-based MOFs.[18] A control experiment with the **(FeTPP)$_2$O** complex resulted in a CO partial current density of 0.72 mA cm$^{-2}$ and a CO selectivity of only 82% (Fig. 6 and Table S5). These results suggest that the presence of the dimeric form alone does not result in significant improvements in catalytic performance for $CO_2$ reduction. Further control experiments with a mixture of **FeTPP** and methyl viologen (**MV**) not only worsened the catalytic activity but also favored the hydrogen evolution reaction (HER) over the $CO_2$RR (Fig. 6). This underscores the importance of covalently attached viologen units in **(FeDVPP)$_2$O** for promoting selectivity towards CO over $H_2$.

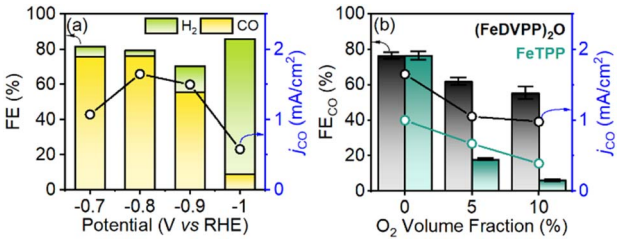


Fig. 5 (a) Faradaic efficiency (FE) and CO partial current density ($j_{CO}$) of heterogenized **(FeDVPP)$_2$O** on the CNT/CP electrode in $CO_2$-saturated 0.5 M $KHCO_3$ after 30 min of electrolysis at different potentials. (b) Comparison of performance of **(FeDVPP)$_2$O** and **FeTPP** after 30 min of electrolysis at −0.8 V *vs.* RHE at different $O_2$ volume fractions (in the $CO_2$ + $O_2$ mixture).

### Aerobic $CO_2$RR catalysis under heterogeneous conditions

We then investigated the $CO_2$RR activity in the presence of $O_2$ under heterogeneous conditions. **(FeDVPP)$_2$O** exhibited a maximum $FE_{CO}$ of 62% and 55% when $CO_2$ was co-fed with 5% $O_2$ and 10% $O_2$, respectively, at an applied potential of −0.8 V (Fig. 5b and Table S5). These values were significantly higher than the $FE_{CO}$ values of 18% and 6% observed for **FeTPP** under similar conditions (Fig. 5b). Another way to assess the catalytic performance is by considering the selectivity for CO production, which is expressed as the ratio of $FE_{CO}$ to global FE. In this case, our data show a CO selectivity of 74% and 63% for **(FeDVPP)$_2$O** when co-feeding $CO_2$ with 5% $O_2$ and 10% $O_2$, respectively. These values are significantly higher than the CO selectivity values of 22% and 8% observed for **FeTPP** under similar conditions. These selectivity results are consistent with the trend observed for $FE_{CO}$.

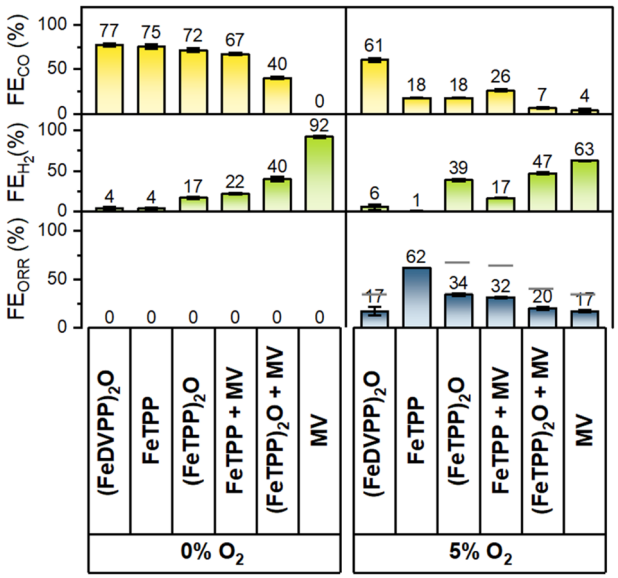


Fig. 6 Faradaic efficiencies (FE) of **(FeDVPP)$_2$O** in comparison to various controls [**FeTPP**, **(FeTPP)$_2$O**, **FeTPP + MV**, **(FeTPP)$_2$O + MV**, and **MV**] after 30 min of electrolysis at −0.8 V *vs.* RHE at 0% and 5% $O_2$ volume fractions. Proper stoichiometries are maintained for accurate comparison of controls relative to **(FeDVPP)$_2$O**. All data are summarized in Table S5. The ORR represents $O_2$ consumption assuming a 2e$^-$ reduction (if 4e$^-$ occurs, the gray bar is expected).

At the optimal potential of −0.8 V, eTOF was calculated to be 5.06 $s^{-1}$ for **(FeDVPP)$_2$O**, a value almost four times that of the **FeTPP** modified electrode (1.32 $s^{-1}$), under anaerobic conditions (Fig. S42). However, under aerobic conditions, eTOF decreased with an increase in $O_2$ percentage and was found to be 3.2 $s^{-1}$ and 3.0 $s^{-1}$ under 5% $O_2$ and 10% $O_2$, respectively, for **(FeDVPP)$_2$O**. This is still relatively higher compared to 0.89 $s^{-1}$ and 0.52 $s^{-1}$ for **FeTPP** under similar conditions. This decrease in eTOF for both **(FeDVPP)$_2$O** and **FeTPP** is consistent with the trend for a decrease in $FE_{CO}$ observed earlier. In addition, the partial current density ($j_{CO}$) of **(FeDVPP)$_2$O** can reach a maximum value of −1.05 mA $cm^{-2}$ at −0.8 V, surpassing the value of −0.67 mA $cm^{-2}$ for **FeTPP** at the same potential when co-feeding $CO_2$ with 5% $O_2$ (Fig. 5b).

An interesting observation concerns the increase in the current density of **FeTPP** with increased $O_2$ content in the $CO_2$ + $O_2$ saturated electrolyte (Fig. S37d and S40) pertaining to the fact that the ORR is promoted in parallel with $CO_2$ reduction and gaining prominence with higher $O_2$ content. However, in the case of **(FeDVPP)$_2$O** modified electrodes, the current density seems to vary marginally irrespective of $O_2$ content (Fig. S37c and S40). This means that on the surface of the electrode, after cleavage of the μ-oxo bond, the reduced forms of **FeDVPP** have a greater selectivity for the $CO_2$RR than ORR. This observation is further supported by the fact that the $j_{ORR}$ of **FeDVPP** (−0.24 mA $cm^{-2}$) is lower compared to the $j_{ORR}$ of **MV** (−0.90 mA $cm^{-2}$), as shown in Table S5. It seems that when adsorbed onto the surface of the graphitic electrode, the reduced Fe(II) species, flanked by the reduced viologen units, become less prone to catalyzing the ORR but exhibit increased activity toward the $CO_2$RR. A plausible explanation for this behavior may lie in the changes to the electronic properties and the resulting spin states of such species (Fig. 4) and consequently the reactivity of these reduced species on the surface of the carbon electrode. As was recently highlighted by calculations on CoTPP adsorbed on graphite surfaces by Hammes-Schiffer and colleagues,[35] the phenyl ring may distort and flatten somewhat in relation to the porphyrin ring. If such structural changes occur on the electrode surface, we expect a reshuffling of electronic properties, which could enhance charge transfer from the reduced viologen to the Fe(II) center, thereby altering the reactivity of the adsorbed **FeDVPP**. The change in solubility and availability of the substrate ($CO_2$ and $O_2$) and co-substrate ($H^+$) under homogeneous (organic) and heterogeneous (aqueous) conditions may have also altered $CO_2$RR and ORR activities as reported previously.[20,36–41] These results, coupled with the enhanced FE for CO, provide strong evidence that **FeDVPP** can sustain the simultaneous reduction of $O_2$. In contrast, the parent **FeTPP** shows a significant decline in electrocatalytic $CO_2$RR performance when $O_2$ is present. Furthermore, we speculate on certain active intermediates of **FeDVPP** that are in constant competition toward the ORR and $CO_2$RR (see Section E of the SI), but further study is required to untangle the complex interplay between these processes and the heterogeneous electron transfers occurring in the reaction layer close to the electrode.

To further interrogate the persistence of **FeDVPP** for the $CO_2$RR in the presence of $O_2$, we performed a series of control experiments (Fig. 6 and Table S5). We synthesized a μ-oxo dimer of **FeTPP**, which we abbreviated as **(FeTPP)$_2$O**[42] and drop-cast on CP. Both **FeTPP** and **(FeTPP)$_2$O** have similar $FE_{CO}$ under anaerobic $CO_2$RR conditions. When co-fed with 5% $O_2$, a significant drop in the $FE_{CO}$ (17%) was observed for both catalysts. Interestingly, we found that the ORR for **FeTPP** was approximately twice that of the **(FeTPP)$_2$O** under our operating conditions (Table S5). It seems that under these conditions the initial face-to-face disposition of **(FeTPP)$_2$O** tends to inhibit the ORR while simultaneously promoting the HER. A similar cooperative effect may also occur in the case of **(FeDVPP)$_2$O**.

We further examined the effect of viologen redox units by investigating **MV** modified electrodes and their admixture with the catalyst FeTPP maintaining proper concentrations for accurate comparison (Fig. 6). Under anaerobic conditions, **MV** mostly produces $H_2$ at an FE of 93%. A similar HER activity of a viologen-based covalent organic framework[43] and methylated diquat[44] has been reported. The HER is also favored for the mixture of **MV** and **FeTPP** or **(FeTPP)$_2$O**. Under a volume fraction of 5% $O_2$ in $CO_2$, the presence of viologen units also affect the ORR of the catalysts, falling from 62% to 35% for **FeTPP** and from 35% to 19% for **(FeTPP)$_2$O** while maintaining a noticeable HER activity. In parallel, the $FE_{CO}$ for the **MV**/**(FeTPP)$_2$O** mixture was significantly diminished, dropping to just 7%. This result supports the benefit of covalently attached viologen units in **(FeDVPP)$_2$O**, as they help decrease not only the ORR but also the HER in the aerobic $CO_2$RR, while maintaining a high $FE_{CO}$.

*Ex situ* X-ray photoelectron spectroscopy (XPS) was conducted on the **(FeDVPP)$_2$O** modified electrodes before and after

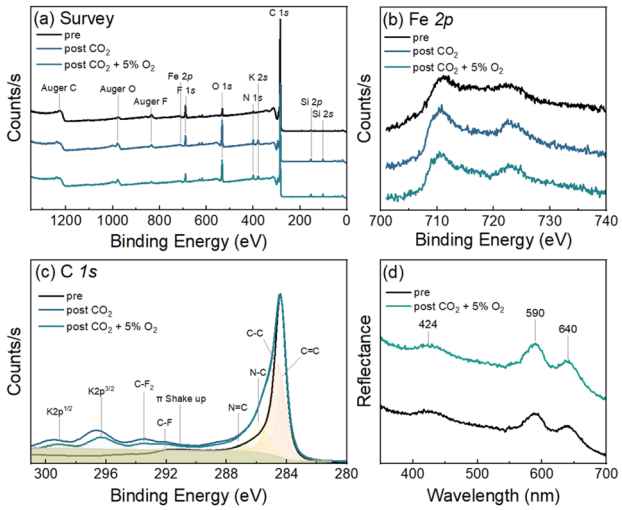


Fig. 7 (a) Survey XPS spectrum, high resolution (b) Fe 2p and (c) C 1s spectra and (d) UV-vis spectra of **(FeDVPP)$_2$O** modified CNT/CP electrodes before and after anaerobic and aerobic (5% $O_2$) $CO_2$RRs.

electrolysis, to investigate if the anaerobic and aerobic $CO_2$RR electrolysis modified the adsorbed catalysts (Fig. 7a–c). The high-resolution XPS spectra of Fe 2p do not show any noticeable alteration in the Fe 2p signals (Fig. 7b). This indicates that the catalyst remains stable after catalysis and even in the presence of any produced $H_2O_2$ (Fig. S9). Additional peaks are observed after electrolysis (Fig. 7a) but correspond to the K 2s, K 2p, and O 1s signals originating from the $KHCO_3$ electrolyte, as well as the Si 2s and Si 2p signals originating from the sintered frit of the electrochemical cell. While the high-resolution XPS spectra of C 1s (Fig. 7c) did not exhibit significant variations, some changes are observed in the N 1s spectra (Fig. S43 and Table S8). A decrease in the $N^+$ ratio to almost 50% of pre-electrolysis conditions suggests the persistence of a monoreduced $V^+$ species during the XPS measurements. While this puzzling observation still remains to be clarified, our data suggest that this monoreduced state of viologen in the FeDVPP catalyst can indeed persist under aerobic conditions (Fig. 3b), as similarly observed in a viologen-based COF.[18] While the C=N–Me peak did not significantly decrease for post-electrolysis under anaerobic $CO_2$RR, we observed a significant decrease under aerobic $CO_2$RR, possibly indicating demetallation. Whether these *ex situ* measurements suggest changes in the molecular understanding of the mechanism or participation of pre-transformed or degraded catalysts remains to be investigated by in-depth *in situ* or *operando* techniques.

## Conclusions

Our results let us to conclude that the improved $CO_2$RR activity, along with the concomitant reduction in the ORR, is achieved possibly through the synergistic features of our viologen-modified iron porphyrin pre-catalyst, **(FeDVPP)$_2$O**. When adsorbed on the MWCNTs/carbon paper electrode, the $CO_2$RR maintained a reasonable $FE_{CO}$ of up to 62% in the presence of 5% of $O_2$ in the feed gas, much surpassing the 7% $FE_{CO}$ achieved from a physical mixture of **FeTPP** or **(FeTPP)$_2$O** with methyl viologen, which resembles the uncoupled components of a bifunctional system. The improvement in performance is not due to the additive effects of separate components but rather to their covalent integration within a unified molecular structure. We speculate that this integration promotes intramolecular electron transfer between the constitutive units forming various intermediates that are in constant competition toward the ORR and $CO_2$RR at different rates. We posit that the additional ORR activity of the viologen groups would lead to increased depletion of $O_2$ in the heterogeneous catalyst layer, which would be beneficial for the $CO_2$RR by the highly reduced states of iron porphyrin, in addition to the advantage of lower concentration of $O_2$ in the aqueous electrolyte of the heterogeneous system.

A more comprehensive mechanistic study in the homogeneous phase is needed to fully understand the impact of partially reduced oxygen species on $CO_2$ activation, such as their influence on the shift to a more positive onset potential for the $CO_2$RR and the much more dominant ORR than the $CO_2$RR. The discerned disparity between homogeneous and heterogeneous catalysis underscores the critical significance of the reaction environment, interfacial organization, catalyst immobilisation, and electron transfer kinetics at the electrode surface. Future mechanistic investigations, especially those utilising *operando*, interface-sensitive spectroscopic methods, will be crucial to comprehensively clarify the interaction between the ORR and $CO_2$RR and to substantiate the suggested function of intramolecular electron transfer in our system.

Our molecular design approach is consistent with the increasing body of work on "$O_2$-tolerant" $CO_2$RR systems (Table S7).[7,9,45–49] However, significant efforts remain necessary to further improve the selective $CO_2$RR in the presence of $O_2$, likely through the integration of various strategies that have been explored to date (*e.g.*, gas diffusion electrode with bipolar membrane,[7] pressurization of feed gas,[47] polymeric filters,[9,46] and reticular frameworks[10,45]). Advancements in this research field will play a pivotal role in making the $CO_2$RR from concentrated $CO_2$ sources more cost-efficient.

## Author contributions

Conceptualization: A. A.; data curation: H. R. and P. G.; investigation: H. R. and D. D.; formal analysis: H. R., P. G., W. L. and A. A.; supervision: P. G. and A. A.; validation: P. G., W. L., and A. A.; writing: all authors contributed to writing and reviewing of the manuscript.

## Conflicts of interest

There are no conflicts to declare.

## Data availability

Upon reasonable request, raw data can be made available from the corresponding author.

The data supporting the findings described in this paper are available within the article and in its Supporting Information (SI). Supplementary information is available. See DOI: **https://doi.org/10.1039/d5sc02722e**.

## Acknowledgements

H. R. was financially supported by the CEA ECC Focus program. This work was also supported by the French Infrastructure for Integrated Structural Biology platform (FRISBI, ANR-10-INSB-05-01) and the French National Agency for Research within the France 2030 plan (Air Capture, ANR-24-RRII-0004). We thank CEA Saclay, CNRS, ICMMO, and University Paris-Saclay for complementary support. Dr Christian Herrero is acknowledged for EPR measurements at ICMMO. A. A. was further supported by Institut Universitaire de France.

## References

1 S. C. Peter, *ACS Energy Lett.*, 2018, **3**, 1557–1561.
2 P. Gotico, Z. Halime and A. Aukauloo, *Dalton Trans.*, 2020, **49**, 2381–2396.
3 S. Amanullah, P. Saha, A. Nayek, M. E. Ahmed and A. Dey, *Chem. Soc. Rev.*, 2021, **50**, 3755–3823.
4 S. Dongare, M. Zeeshan, A. S. Aydogdu, R. Dikki, S. F. Kurtoğlu-Öztulum, O. K. Coskun, M. Muñoz, A. Banerjee, M. Gautam, R. D. Ross, J. S. Stanley, R. S. Brower, B. Muchharla, R. L. Sacci, J. M. Velázquez, B. Kumar, J. Y. Yang, C. Hahn, S. Keskin, C. G. Morales-Guio, A. Uzun, J. M. Spurgeon and B. Gurkan, *Chem. Soc. Rev.*, 2024, **53**, 8563–8631.
5 E. Lamy, L. Nadjo and J. M. Saveant, *J. Electroanal. Chem. Interf. Electrochem.*, 1977, **78**, 403–407.
6 B. Mondal, P. Sen, A. Rana, D. Saha, P. Das and A. Dey, *ACS Catal.*, 2019, **9**, 3895–3899.
7 D. J. D. Pimlott, A. Jewlal, Y. Kim and C. P. Berlinguette, *J. Am. Chem. Soc.*, 2023, **145**, 25933–25937.
8 M. S. Prévot, V. Finelli, X. Carrier, G. Deplano, M. Cavallo, E. A. Quadrelli, J. Michel, M.-H. Pietraru, C. Camp, G. Forghieri, A. Gagliardi, S. Seidel, A. Missemer, B. Reuillard, B. Centrella, S. Bordiga, M. G. S. González, V. Artero, K. V. A. Birkelbach and N. von Wolff, *Chem. Sci.*, 2024, **15**, 9054–9086.
9 X. Lu, Z. Jiang, X. Yuan, Y. Wu, R. Malpass-Evans, Y. Zhong, Y. Liang, N. B. McKeown and H. Wang, *Sci. Bull.*, 2019, **64**, 1890–1895.
10 H. Guo, D.-H. Si, H.-J. Zhu, Z.-A. Chen, R. Cao and Y.-B. Huang, *Angew. Chem., Int. Ed.*, 2024, **63**, e202319472.
11 S. Dey, B. Mondal, S. Chatterjee, A. Rana, S. Amanullah and A. Dey, *Nat. Rev. Chem.*, 2017, **1**, 1–20.
12 Y. Gao, X. Xu, Y. Niu, X. Hu, Z. Li, L. Yang, L. Zhi and B. Wang, *Nano Res.*, 2023, **16**, 12936–12941.
13 Q. Lin, Q. Li, C. Batchelor-McAuley and R. G. Compton, *J. Electrochem. Sci. Technol.*, 2013, **4**, 71–80.
14 L. Chen, C. Lin and R. G. Compton, *Phys. Chem. Chem. Phys.*, 2018, **20**, 15795–15806.
15 M. Kathiresan, B. Ambrose, N. Angulakshmi, D. E. Mathew, D. Sujatha and A. M. Stephan, *J. Mater. Chem. A*, 2021, **9**, 27215–27233.
16 C. Costentin, D. G. Nocera and C. N. Brodsky, *Proc. Natl. Acad. Sci. U. S. A.*, 2017, **114**, 11303–11308.
17 C. P. Andrieux, P. Hapiot and J. M. Savéant, *J. Electroanal. Chem. Interf. Electrochem.*, 1985, **189**, 121–133.
18 Y.-L. Dong, Z.-Y. Jing, Q.-J. Wu, Z.-A. Chen, Y.-B. Huang and R. Cao, *J. Mater. Chem. A*, 2023, **11**, 8739–8746.
19 K. M. Kadish, G. Larson, D. Lexa and M. Momenteau, *J. Am. Chem. Soc.*, 1975, **97**, 282–288.
20 A. Haryono, K. Oyaizu, K. Yamamoto, J. Natori and E. Tsuchida, *Chem. Lett.*, 1998, **27**, 233–234.
21 K. Oyaizu, A. Haryono, J. Natori, H. Shinoda and E. Tsuchida, *Bull. Chem. Soc. Jpn.*, 2000, **73**, 1153–1163.
22 A. Fidalgo-Marijuan, G. Barandika, B. Bazán, M. K. Urtiaga, E. S. Larrea, M. Iglesias, L. Lezama and M. I. Arriortua, *Dalton Trans.*, 2014, **44**, 213–222.
23 P. Gotico, Z. Halime, W. Leibl and A. Aukauloo, *ChemPlusChem*, 2023, **88**, e202300222.
24 I. Garcia-Bosch, S. K. Sharma and K. D. Karlin, *J. Am. Chem. Soc.*, 2013, **135**, 16248–16251.
25 D. M. Harraz, S. Weng and Y. Surendranath, *ACS Catal.*, 2023, **13**, 1462–1469.
26 S. Amanullah, P. Gotico, M. Sircoglou, W. Leibl, M. J. Llansola-Portoles, T. Tibiletti, A. Quaranta, Z. Halime and A. Aukauloo, *Angew. Chem., Int. Ed.*, 2024, **63**, e202314439.
27 E. Pugliese, P. Gotico, I. Wehrung, B. Boitrel, A. Quaranta, M.-H. Ha-Thi, T. Pino, M. Sircoglou, W. Leibl, Z. Halime and A. Aukauloo, *Angew. Chem., Int. Ed.*, 2022, **61**, e202117530.
28 D. H. Cruz Neto, E. Pugliese, P. Gotico, A. Quaranta, W. Leibl, K. Steenkeste, D. Peláez, T. Pino, Z. Halime and M.-H. Ha-Thi, *Angew. Chem., Int. Ed.*, 2024, **63**, e202407723.
29 C. Römelt, J. Song, M. Tarrago, J. A. Rees, M. van Gastel, T. Weyhermüller, S. DeBeer, E. Bill, F. Neese and S. Ye, *Inorg. Chem.*, 2017, **56**, 4745–4750.
30 W. W. Porter and T. P. Vaid, *J. Org. Chem.*, 2005, **70**, 5028–5035.
31 M. Abdinejad, C. Dao, B. Deng, M. E. Sweeney, F. Dielmann, X. Zhang and H. B. Kraatz, *ChemistrySelect*, 2020, **5**, 979–984.
32 C. Zhang, P. Gotico, R. Guillot, D. Dragoe, W. Leibl, Z. Halime and A. Aukauloo, *Angew. Chem., Int. Ed.*, 2023, **62**, e202214665.
33 C. Zhang, D. Dragoe, F. Brisset, B. Boitrel, B. Lassalle-Kaiser, W. Leibl, Z. Halime and A. Aukauloo, *Green Chem.*, 2021, **23**, 8979–8987.
34 S. Chowdhury, Y. Nassar, L. Guy, D. Frath, F. Chevallier, E. Dumont, A. P. Ramos, G. J.-F. Demets and C. Bucher, *Electrochim. Acta*, 2019, **316**, 79–92.
35 P. Hutchison, C. J. Kaminsky, Y. Surendranath and S. Hammes-Schiffer, *ACS Cent. Sci.*, 2023, **9**, 927–936.
36 M. L. Rigsby, D. J. Wasylenko, M. L. Pegis and J. M. Mayer, *J. Am. Chem. Soc.*, 2015, **137**, 4296–4299.
37 C. Costentin, H. Dridi and J.-M. Savéant, *J. Am. Chem. Soc.*, 2015, **137**, 13535–13544.

38 M. N. Jackson, C. J. Kaminsky, S. Oh, J. F. Melville and Y. Surendranath, *J. Am. Chem. Soc.*, 2019, **141**, 14160–14167.
39 C. J. Kaminsky, S. Weng, J. Wright and Y. Surendranath, *Nat. Catal.*, 2022, **5**, 430–442.
40 M. L. Clark, A. Ge, P. E. Videla, B. Rudshteyn, C. J. Miller, J. Song, V. S. Batista, T. Lian and C. P. Kubiak, *J. Am. Chem. Soc.*, 2018, **140**, 17643–17655.
41 A. Morozan, S. Campidelli, A. Filoramo, B. Jousselme and S. Palacin, *Carbon*, 2011, **49**, 4839–4847.
42 E. B. Fleischer and T. S. Srivastava, *J. Am. Chem. Soc.*, 1969, **91**, 2403–2405.
43 S. Altınışık, G. Yanalak, İ. Hatay Patır and S. Koyuncu, *ACS Appl. Mater. Interfaces*, 2023, **15**, 18836–18844.
44 K. Kawano, K. Yamauchi and K. Sakai, *Chem. Commun.*, 2014, **50**, 9872–9875.
45 H.-J. Zhu, D.-H. Si, H. Guo, Z. Chen, R. Cao and Y.-B. Huang, *Nat. Commun.*, 2024, **15**, 1479.
46 P. Li, X. Lu, Z. Wu, Y. Wu, R. Malpass-Evans, N. B. McKeown, X. Sun and H. Wang, *Angew. Chem., Int. Ed.*, 2020, **59**, 10918–10923.
47 Y. Xu, J. P. Edwards, J. Zhong, C. P. O'Brien, C. M. Gabardo, C. McCallum, J. Li, C.-T. Dinh, E. H. Sargent and D. Sinton, *Energy Environ. Sci.*, 2020, **13**, 554–561.
48 H. Shi, H. Pan, Y. Cheng, S. Lu and P. Kang, *Chemelectrochem*, 2021, **8**, 1792–1797.
49 Y. Cheng, J. Hou and P. Kang, *ACS Energy Lett.*, 2021, **6**, 3352–3358.